PROPERTIES OF PHASE SHIFT DEFECTS IN ONE-DIMENSIONAL RUGATE PHOTONIC STRUCTURES

Y. Y. Liu

College of Physical Sciences and Technology
Sichuan University, Chengdu, Sichuan 610065, China

Z. Lu

Cornell University
Ithaca, NY 14853, USA

Abstract—We theoretically investigated optical properties of phase shift defects in one-dimensional rugate photonic structures at oblique incidence. Transmission spectra and energy density distributions of such continuous gradient-index structures with phase shift defects were numerically calculated for TE and TM waves using the propagation matrix method. The study shows that when the angle of incidence increases, (1) the wavelength of the defect mode shifts to a shorter wavelength, (2) the stop band of the rugate structure moves toward a shorter wavelength region, (3) the bandwidth is enlarged for TE wave, but it is shortened for TM wave, (4) the full width at half maximum (FWHM) of the defect mode decreases for TE wave but it increases for TM wave, (5) the peak energy density increases and then drops for TE wave, while it always decreases for TM wave. The effect of number of periods of rugate structures on the energy density distribution was also examined.

1. INTRODUCTION

One-dimensional photonic crystals are composed of materials with a periodic index of refraction in only one direction [1]. The photonic band gaps of these structures provide a way to control the propagation of light within a range of frequency [2–11], for example, an omnidirectional reflector has been demonstrated using

one-dimensional periodic dielectric materials [5, 6, 12–14]. One-dimensional rugate photonic structures, which have a sinusoidal variation of the refractive index, have been used as optical interference filters [15] and environmental sensors [16]. To further control the light within the photonic band gaps of rugate structures, defects are introduced, i.e., the refractive index is locally modified. This has been shown in recent studies using the glancing angle deposition technique (GLAD) [15, 17–21]. On the basis of oblique thin structure deposition and substrate rotation, GLAD is able to fabricate continuous gradient-index structures with localized defects at micro- or nano-scale in a *one-step* way using a single optical material [15, 17–21].

A phase shift defect centered in a one-dimensional rugate structure as a narrow bandpass filter has been fabricated using GLAD [18, 20]. In the case of normal incidence, experimental transmission spectra were measured, and compared to theoretical transmission spectra calculated by a characteristic matrix method using a very thin (1 nm) layer approximation [18]. Although optical properties of such a phase shift defect mode are also important and interesting under oblique incidence [18, 20], both experimental and theoretical studies so far have not been reported. The purpose of this study was to theoretically investigate optical properties of phase shift defects in a one-dimensional rugate structure at oblique incidence using an efficient propagation matrix method [22]. We numerically calculated transmission spectra and energy density distributions for TE and TM waves, and analyzed changes of transmission spectra and energy density distributions when the angle of incidence increases. This study may provide a better understanding of designing narrow bandpass filters or optical amplifiers using one-dimensional continuous gradient-index optical materials.
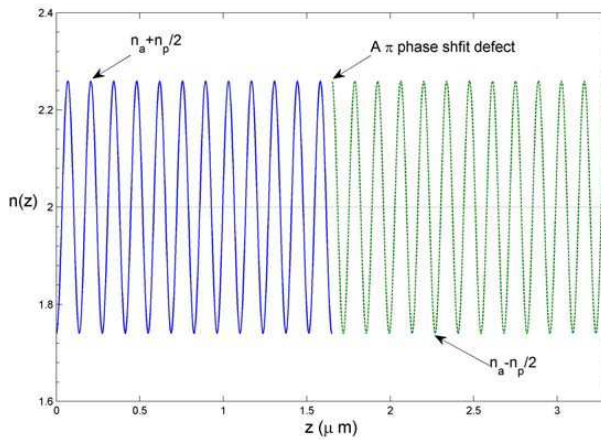
2. THE MODEL AND METHODS

The refractive index profile of the rugate structure with a phase shift defect in the middle is described by [18],

$$
n(z) = \begin{cases} n_a + \frac{n_p}{2} \sin\left(\frac{4\pi n_a}{\lambda_0} z + \alpha_0\right), & z \in \left[0, \ \frac{d}{2}\right] \\ n_a + \frac{n_p}{2} \sin\left(\frac{4\pi n_a}{\lambda_0} z + \alpha_0 + \alpha\right), & z \in \left[\frac{d}{2}, \ d\right] \end{cases} . \qquad (1)
$$

The average and modulation indexes are denoted by n_a and n_p, respectively; the designed wavelength of the rugate structure, λ_0, is located within the photonic band gap; the phase angle at $z = 0$ and the phase shift angle of the defect are represented by α_0 and α, respectively.

The refractive index profile of a 24-period rugate structure with a π phase shift defect in the center is illustrated in Figure 1. The plane of incidence was assumed to be the x-z plane, and the angle of incidence, θ, is determined by the angle between z direction and the direction of light incident on the interface at $z = 0$. The monochromatic light was assumed to be incident from air and outgoing from glass. Parameter values and definitions used in calculation are listed in Table 1.

To calculate transmittance and reflectance of one-dimensional rugate structures, the coupled-mode theory and the 2×2 transfer

Figure 1. The refractive index profile of a rugate structure with a π phase shift defect in the center ($\alpha_0 = -90°$).

Table 1. Parameters used in calcualtions.

Symbol	Value	Definition
λ_0	550 nm	Designed wavelength of the rugate structure
n_a	2.0	Average refractive index
n_p	0.52	Modulation (perturbation) index
n_i	1.0	The incident medium (air)
n_t	1.53	The outgoing medium (glass)
p	137.5 nm	Period of the rugate structure
d	3.3 µm	Length of the rugate structure, $d = 24p$
α	0°–360°	Phase shift angle
θ	0°–90°	The angle of incidence

(propagation) matrix method [23–25] have been commonly used. When the modulation (perturbation) index (n_p) is small, $n_p \ll n_a$, the coupled-mode theory is able to have accurate calculations [23, 24]. While the 2×2 transfer matrix method generally does not have such a restriction, numerical calculations of propagation matrices are required, using a layer approximation that divides the whole structure into many small layers so that each inhomogeneous layer is approximately homogeneous. Accurately numerical calculations using the propagation (characteristic) matrix method for a rugate structure with a phase shift defect needs many thin layers, for example, a layer thickness of 1 nm [18]. This may be inconvenient and time-consuming when we want to examine the effects of different parameter values on transmittance and reflectance. In our previous work, we have developed an efficient propagation matrix method for anisotropic and inhomogeneous (smoothly varying index) optical media [22]. On the basis of [26] by Abdulhalim and [27–29] by Chin et al., we constructed an efficient fourth-order symplectic propagation matrix and compared its efficiency to the commonly used second-order propagation (transfer or characteristic) matrix for a cholesteric liquid crystal [22]. Although the developed efficient algorithm is for anisotropic and inhomogeneous optical materials, as a matter of fact, the fourth-order symplectic propagation matrix is also applied for isotropic and inhomogeneous structures such as rugate structures.

For isotropic optical materials, the 4×4 propagation matrix is decoupled into two 2×2 propagation matrices for TE and TM waves [22, 26, 30]. The electromagnetic fields inside a rugate structure for TE and TM waves follow:

$$\frac{d}{dz} \begin{pmatrix} E_y \\ -\eta_0 H_x \end{pmatrix} = ik_0 \Delta_s(z) \begin{pmatrix} E_y \\ -\eta_0 H_x \end{pmatrix}$$

$$= ik_0 \begin{pmatrix} 0 & 1 \\ \varepsilon(z) - (n_i \sin\theta)^2 & 0 \end{pmatrix} \begin{pmatrix} E_y \\ -\eta_0 H_x \end{pmatrix}, \text{ TE wave} \qquad (2)$$

$$\frac{d}{dz} \begin{pmatrix} E_x \\ \eta_0 H_y \end{pmatrix} = ik_0 \Delta_p(z)$$

$$= ik_0 \begin{pmatrix} 0 & 1 - \frac{(n_i \sin\theta)^2}{\varepsilon(z)} \\ \varepsilon(z) & 0 \end{pmatrix} \begin{pmatrix} E_x \\ \eta_0 H_y \end{pmatrix}, \text{ TM wave} \qquad (3)$$

where the dielectric permittivity, the angle of incidence, the index of medium of the monochromatic light incident from, the vacuum wave number, and the impedance of a vacuum are denoted by $\varepsilon(z)$, θ, n_i, k_0, and η_0, respectively. To solve Eqs. (2) and (3), the rugate structure are assumed to be sliced into N layers with a layer thickness $h = N/d$, and therefore the formal solutions of Eqs. (2) and (3) for a layer between

z_j and $z_{j+1} = z_j + h$ $(j = 0 - N,\ z_N = z_d)$ are:

$$\begin{pmatrix} E_y(z_{j+1}) \\ -\eta_0 H_x(z_{j+1}) \end{pmatrix} = T \left\{ \exp \left(ik_0 \int_{z_j}^{z_{j+1}} \Delta_s(z) dz \right) \right\} \begin{pmatrix} E_y(z_j) \\ -\eta_0 H_x(z_j) \end{pmatrix}, \text{ TE wave } (4)$$

$$\begin{pmatrix} E_x(z_{j+1}) \\ \eta_0 H_y(z_{j+1}) \end{pmatrix} = T \left\{ \exp \left(ik_0 \int_{z_j}^{z_{j+1}} \Delta_p(z) dz \right) \right\} \begin{pmatrix} E_x(z_j) \\ \eta_0 H_y(z_j) \end{pmatrix}, \text{ TM wave } (5)$$

where the space-ordering operator is denoted by T. Analytical expressions of the exponent matrix operators in Eqs. (4) and (5) are generally not available for most gradient-index materials, therefore, layer approximation has to be applied. When the layer thickness is small enough, the formal solutions are approximated as,

$$\begin{pmatrix} E_y(z_{j+1}) \\ -\eta_0 H_x(z_{j+1}) \end{pmatrix} = \exp(ik_0 h \Delta_s(z + h/2)) \begin{pmatrix} E_y(z_j) \\ -\eta_0 H_x(z_j) \end{pmatrix}$$

$$= \begin{pmatrix} \cos(k_0 h\varsigma) & \frac{i\sin(k_0 h\varsigma)}{\varsigma} \\ i\varsigma \sin(k_0 h\varsigma) & \cos(k_0 h\varsigma) \end{pmatrix} \begin{pmatrix} E_y(z_j) \\ -\eta_0 H_x(z_j) \end{pmatrix}$$

$$= P_{2s}(z_{j+1}, z_j) \begin{pmatrix} E_y(z_j) \\ -\eta_0 H_x(z_j) \end{pmatrix}, \text{ TE wave } \qquad (6)$$

$$\begin{pmatrix} E_x(z_{j+1}) \\ \eta_0 H_y(z_{j+1}) \end{pmatrix} = \exp(ik_0 h \Delta_p(z + h/2)) \begin{pmatrix} E_x(z_j) \\ \eta_0 H_y(z_j) \end{pmatrix}$$

$$= \begin{pmatrix} \cos(k_0 h\varsigma) & \frac{i\varsigma \sin(k_0 h\varsigma)}{\varepsilon(z_j + h/2)} \\ \frac{i\varepsilon(z_j + h/2)\sin(k_0 h\varsigma)}{\varsigma} & \cos(k_0 h\varsigma) \end{pmatrix} \begin{pmatrix} E_x(z_j) \\ \eta_0 H_y(z_j) \end{pmatrix}$$

$$= P_{2p}(z_{j+1}, z_j) \begin{pmatrix} E_x(z_j) \\ \eta_0 H_y(z_j) \end{pmatrix}, \text{ TM wave } \qquad (7)$$

where the eigenvalue $\varsigma = (\varepsilon(z_j + h/2) - (n_i \sin\theta)^2)^{1/2}$. In our previous study [31, 32], we have showed that the propagation matrices, P_{2s} and P_{2p}, in Eqs. (6) and (7) are only correct up to the second order of the layer thickness (h). In this study, a fourth-order symplectic integrator [22, 27–29, 33] for the layer propagation matrices was used

to approximate the formal solutions (Eqs. (3) and (4)),

$$\begin{pmatrix} E_y(z_{j+1}) \\ -\eta_0 H_x(z_{j+1}) \end{pmatrix}$$

$$= e^{ik_0 h b_1 \Delta_s(z_j+t_3 h)} e^{ik_0 h b_2 \Delta_s(z_j+t_2 h)} e^{ik_0 h b_1 \Delta_s(z_j+t_1 h)} \begin{pmatrix} E_y(z_j) \\ -\eta_0 H_x(z_j) \end{pmatrix}$$

$$= P_{4s}(z_{j+1}, z_j) \begin{pmatrix} E_y(z_j) \\ -\eta_0 H_x(z_j) \end{pmatrix}, \text{ TE wave} \tag{8}$$

$$\begin{pmatrix} E_x(z_{j+1}) \\ \eta_0 H_y(z_{j+1}) \end{pmatrix}$$

$$= e^{ik_0 h b_1 \Delta_p(z_j+t_3 h)} e^{ik_0 h b_2 \Delta_p(z_j+t_2 h)} e^{ik_0 h b_1 \Delta_p(z_j+t_1 h)} \begin{pmatrix} E_x(z_j) \\ \eta_0 H_y(z_j) \end{pmatrix}$$

$$= P_{4p}(z_{j+1}, z_j) \begin{pmatrix} E_x(z_j) \\ \eta_0 H_y(z_j) \end{pmatrix}, \text{ TM wave} \tag{9}$$

where $b_1 = 1/(2-s)$, $b_2 = -s/(2-s)$, $t_1 = 1/(2(2-s))$, $t_2 = 1/2$, $t_3 = 1/2 - (s-1)/(2(2-s))$, and $s = 2^{1/3}$. To evaluate the transmittance and reflectance, we have to find the electromagnetic fields at z_d, which are propagated from z_0,

$$\begin{pmatrix} E_y(z_d) \\ -\eta_0 H_x(z_d) \end{pmatrix} = \prod_{j=0}^{N-1} P_{4s}(z_{j+1}, z_j) \begin{pmatrix} E_y(z_0) \\ -\eta_0 H_x(z_0) \end{pmatrix}, \text{ TE wave} \tag{10}$$

$$\begin{pmatrix} E_x(z_d) \\ \eta_0 H_y(z_d) \end{pmatrix} = \prod_{j=0}^{N-1} P_{4p}(z_{j+1}, z_j) \begin{pmatrix} E_x(z_0) \\ \eta_0 H_y(z_0) \end{pmatrix}. \text{ TM wave} \tag{11}$$

The efficient algorithm for calculating layer propagation matrix correct up to the fourth-order of the layer thickness enables us using a larger layer thickness without sacrificing accuracy; this study assumed 10 layers per period, i.e., $h = 13.75$ nm. The reflectance and transmittance with boundary conditions of electromagnetic fields at z_0 and z_d, therefore, are,

$$R = \frac{|E_{xr}|^2 + \cos^2 \theta |E_{yr}|^2}{|E_{xi}|^2 + \cos^2 \theta |E_{yi}|^2}, \tag{12}$$

$$T = \frac{n_t \cos \theta_t \left(|E_{xt}|^2 / \cos^2 \theta_t + |E_{yt}|^2 \right)}{n_i \cos \theta \left(|E_{xi}|^2 / \cos^2 \theta + |E_{yi}|^2 \right)}, \tag{13}$$

where the index and the refractive angle of the outgoing medium are n_t and θ_t, respectively.

The electromagnetic density distributions are usually calculated by the finite element method [34], but here we calculated them using

the following formulae [24] with the help of the efficient propagation matrix method,

$$Energy\ Density \propto \left(\varepsilon(z)|E_y|^2+|H_x|^2+(n_i\sin\theta)^2|E_y|^2\right), \text{TE wave} \quad (14)$$

$$Energy\ Density \propto \left(\varepsilon(z)\left(|E_x|^2+\left(\frac{n_i\sin\theta}{\varepsilon(z)}\right)^2|H_y|^2\right)+|H_y|^2\right),$$

$$\text{TMwave} \quad (15)$$

To calculate the electromagnetic fields at each position z, we first calculated the propagation matrix at each position, and then applied the propagation matrix to find the reflected electromagnetic fields at $z = 0$. After that, we used the stored propagation matrix to advance the electromagnetic fields from $z = 0$ to $0 < z \le d$. The energy density distributions across the rugate structure were calculated at defect wavelengths for different angles of incidence.

3. NUMERICAL RESULTS AND DISCUSSION

Transmittance of a rugate structure without a phase shift defect at normal incidence is illustrated in Figure 2. When the number of periods (cycles) increases from 4 to 30, we find that a photonic stop band is established. The designed wavelength $\lambda_0 = 550$ nm is close to the center of the stop band, and the bandwidth is about 78 nm.
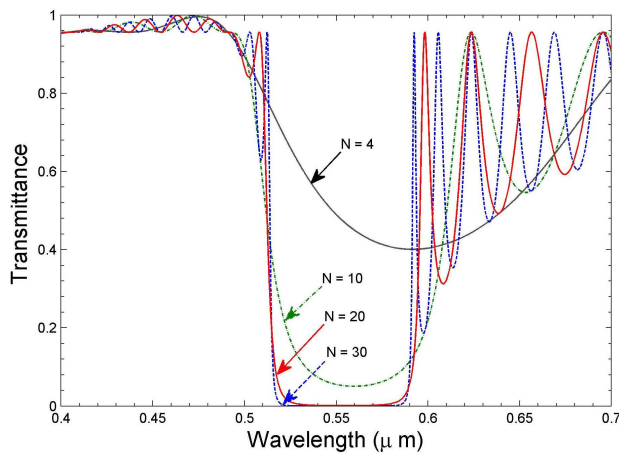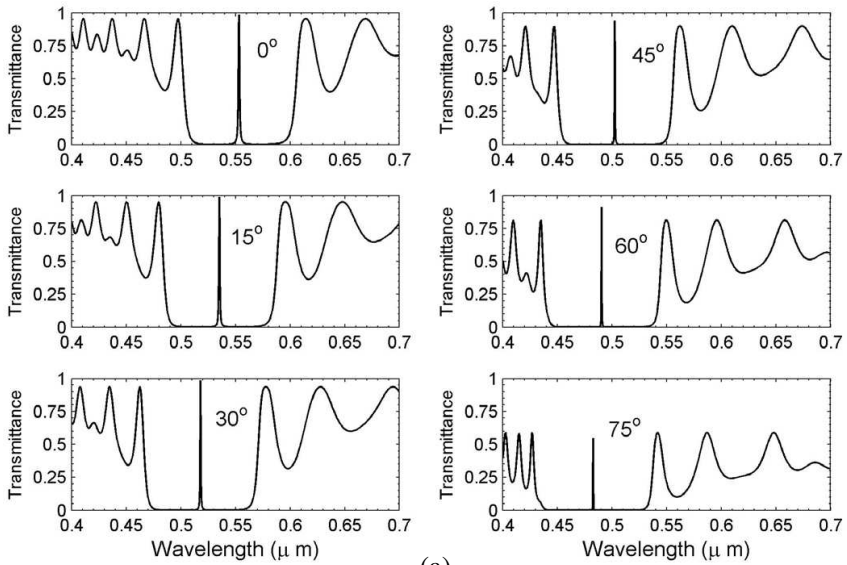

Figure 2. Transmittance of a rugate structure without defects at normal incidence ($\alpha_0 = -90°$); the photonic band gap is established when the number of periods (cycles) increases from 4 to 30.

Figures 3(a) and (b) show transmittance of a π phase shift defect centered in a 24-period ruagte structure with six different angles of incidence, $0°$, $15°$, $30°$, $45°$, $60°$, and $75°$ for TE and TM waves, respectively. At normal incidence, there is no difference between TE and TM waves, and the defect wavelength, $\lambda_{def} = 553\,\text{nm}$, is very close to the designed wavelength, $\lambda_0 = 550\,\text{nm}$. When the angle of incidence increases, for both TE and TM waves, the defect wavelength, λ_{def}, shifts to a shorter wavelength, and the stop band moves toward a range of short wavelengths. The width of stop band for TE wave is enlarged, but for TM wave it is shortened. The peak (resonant) transmittance, for both TE and TM waves, is close to 1 as the angle of incidence increases from $0°$ to $60°$; at the large angle of incidence, for example, $75°$, it reduces to 0.5 for TE wave but is still close to 1 for TM wave. The sharp resonant transmittance due to the introduction of a π phase shift defect provides a narrow pass band — a narrow bandpass filter, and at oblique incidence, the narrow bandpass filter is able to filter different wavelengths. When the angle of incidence increases, for TE wave, the narrow passband becomes even narrower (Figure 3(a)), which suggests that the full width at half maximum (FWHM) decreases; while for TM wave, the narrow passband becomes broader (Figure 3(b)), which means that FWHM increases.

Energy density distributions inside the rugate structure with a π phase shift defect in the middle at the defect wavelength for TE and TM waves are shown in Figures 4(a) and (b), respectively. When the angle of incidence increases, for TE wave (Figure 4 (a)), the peak energy density increases at the defect position, $z_{d/2} = 1.65\,\mu\text{m}$ for a 24-period structure; for TM wave (Figure 4(b)), the overall energy density profile decreases for a 24-period structure. To further look at the subtle difference between TE and TM waves, the maximal energy density against different angles of incidence is plotted in Figure 5. We find that when the angle of incidence increases, for TE wave, the maximal energy density located at the defect wavelength increases and then starts to drop until $\theta = 60°$; for TM wave, the maximal energy density always decreases. Similar finding is observed for a 40-period structure (Figures 4 and 5); however, the magnitude of peak energy density at the defect wavelength for different angles of incidence is nearly 10 — 100 times higher than that of a 20-period structure. The energy density distribution indicates that the localization of light occurs at the center (defect position) of the rugate structure, if the wavelength of the incident light is equal to the defect wavelength. This may provide potential applications for optical amplifiers and nonlinear optics.

The angle dependence of the defect wavelengths and the blue shift of stop bands for TE and TM waves may be qualitatively understood
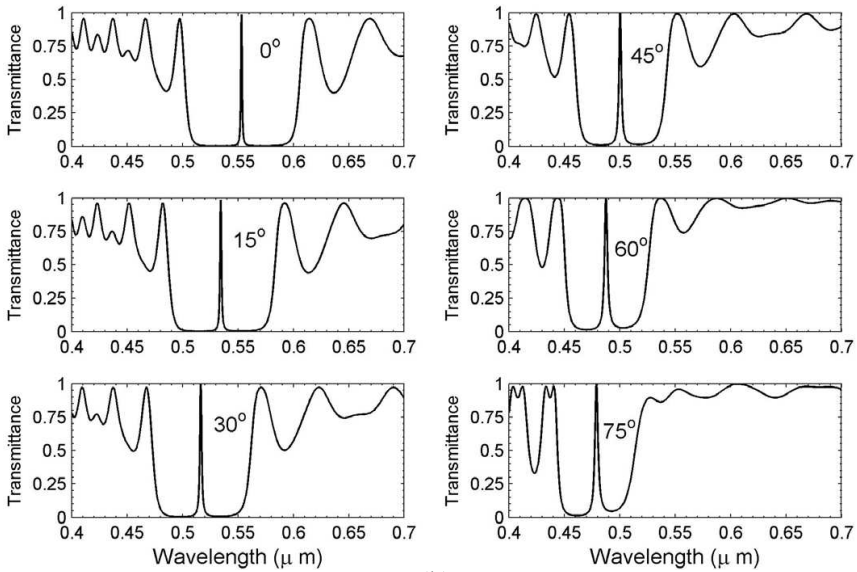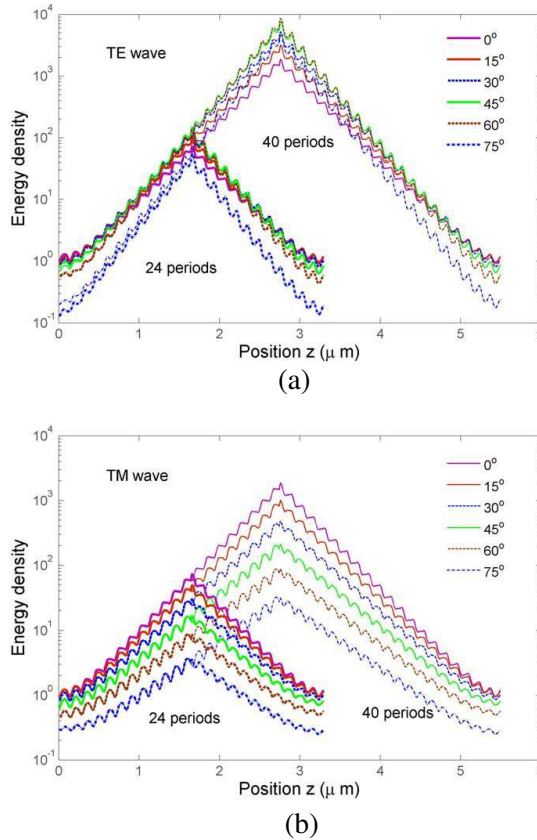
Figure 3. Transmittance of TE (a) and TM (b) waves at different angles of incidence, $\theta = 0°$, $15°$, $30°$, $45°$, $60°$, $75°$.

Figure 4. Energy density profile across the rugate structure with a π phase shift defect at different angles of incidence for (a) TE and (b) TM waves.

based on the coupled-mode theory to a rugate film without a phase shift defect [23]. However we would like to point out that currently there are no exact analytical expressions for reflectance and transmittance for a rugate structure even in the absence of phase shift defects and in the case of normal incidence, and this may limit our ability to give an accurate explanation. The shift of the design wavelength (λ_θ) is related to the angle of incidence (θ) and the original design wavelength (λ_0) via $\lambda_\theta = \lambda_0 (1 - \frac{\sin^2 \theta}{n_a^2})^{1/2}$ [23]. When increasing the angle of incidence (θ), λ_θ becomes smaller than λ_0 and thereby the design wavelength has a blue shift. For the rugate structure with a π phase shift defect in the
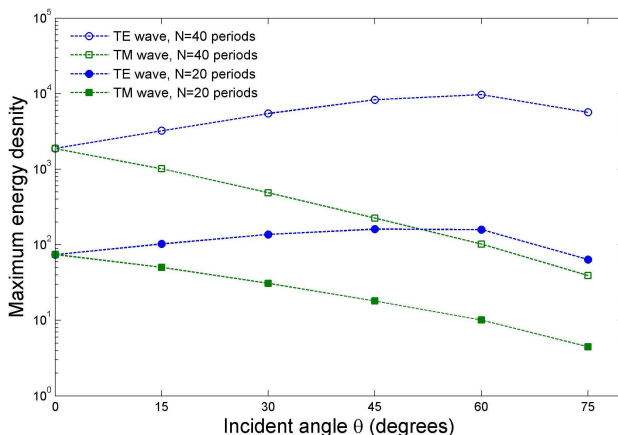
Figure 5. The maximum energy density in the middle (defect position) of the rugate structure against different angles of incidence for TE and TM waves.
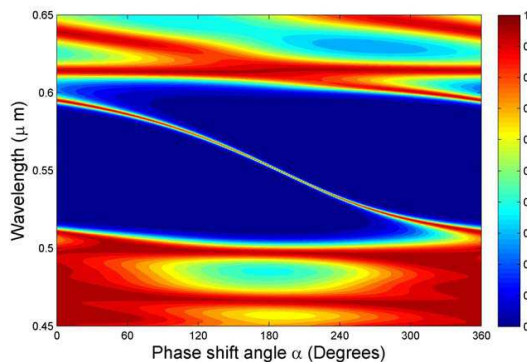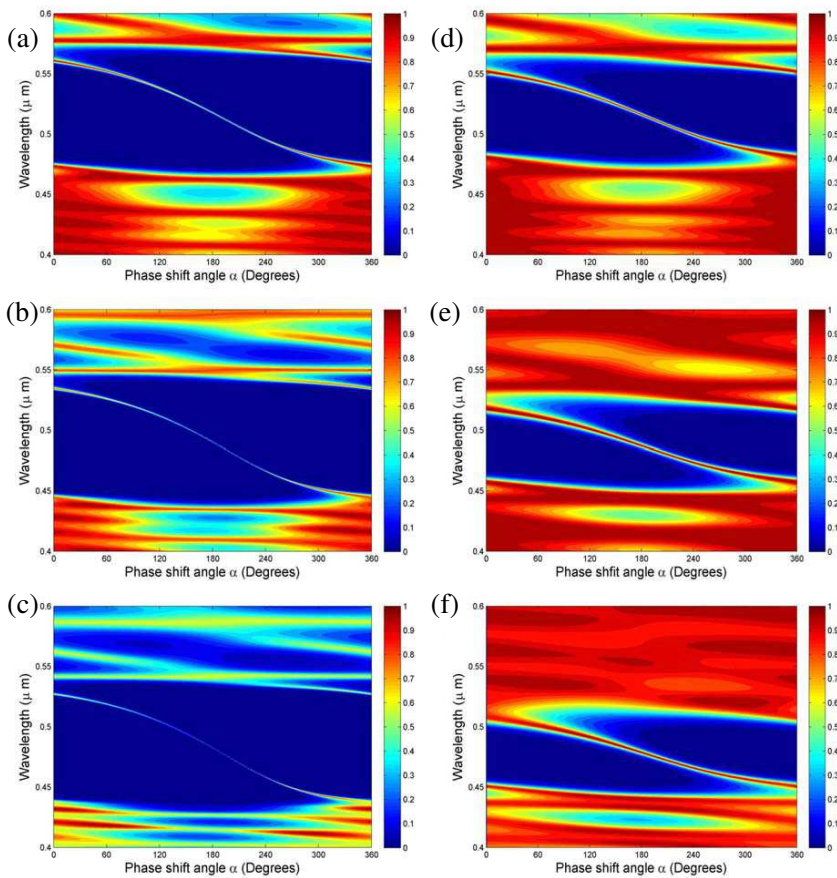

Figure 6. Contour plot of transmittance at normal incidence with respect to a varying phase shift angle ($\alpha \in [0°, 360°]$).

middle, because the defect wavelength (λ_d) is very close to the design wavelength, the λ_d is expected to have a similar shift tendency as the λ_0 when the angle of incidence increases. This may explain the blue shift behavior for the defect wavelength as well as the blue shift of the rugate stop band. The full forbidden bandwidths for a rugate structure without a phase shift defect for TE and TM waves are [23], $\Delta\lambda = \lambda_0(\frac{n_p}{2n_a})(1 - \frac{\sin^2\theta}{n_a^2})^{-1/2}$ and $\Delta\lambda = \lambda_0(\frac{n_p}{2n_a})(1 - \frac{2\sin^2\theta}{n_a^2})(1 - \frac{\sin^2\theta}{n_a^2})^{-1/2}$,

respectively. These expressions clearly explain that when the angle of
incidence (θ) increases, the bandwidth for TE wave is enlarged and for
TM wave it is shortened.

Since the transmitted energy decreases with the increasing angle
of incidence, the peak transmittance of the defect mode for TE wave
slowly decreases. This is a similar result as illustrated in a study for
one-dimensional photonic crystals [8]. However, for TM wave, the peak
transmittance of the defect mode does not show the Brewster angle
effect — the peak transmittance decreases rapidly when the angle of

Figure 7. Contour plot of transmittance at oblique incidence
with respect to a varying phase shift angle ($\alpha \in [0°, 360°]$). The
transmittance for TE wave is shown in (a) $\theta = 30°$, (b) $\theta = 60°$,
(c) $\theta = 75°$, and for TM wave in (d) $\theta = 30°$, (e) $\theta = 60°$, (f) $\theta = 75°$.

incidence is beyond the Brewster angle. This is different from the study in one-dimensional discrete binary photonic multilayer systems [8], because the index of rugate structure varies continuously and the average index is relatively high. The angle dependence patterns of energy densities for TE and TM waves in the rugate structure may be physically understood in terms of group velocity of the propagation of light at defect wavelength with different incident angles, because the group velocity is inversely related to the energy density. For TE wave, when the angle of incidence increases, the group velocity decreases at the defect wavelength and thus the energy density at the rugate center increases; while for TM wave the group velocity monotonically increases, the energy density at the defect position decreases with the increasing angle of incidence.

To examine the effects of the defect in the rugate structure with different phase shifts, contour plots of transmittance are illustrated in Figures 6 (normal incidence) and Figure 7 (oblique incidence, $\theta = 30°$, $60°$, $75°$; Figures 6(a)–(c) for TE wave and (d)–(e) for TM wave). When the phase shift angle (α) increases from $0°$ to $360°$, in Figure 6 (normal incidence, $\theta = 0°$), we find that the defect wavelength shifts from the right edge (the longer wavelength) of the stop band to the left edge (the shorter wavelength), and the shape of transmittance near the π phase shift becomes very sharp. In case of oblique incidence, we find that, when the angle of incidence (θ) increases from $30°$ to $60°$, $75°$ (Figures 7(a)–(c)), for all phase shift angles ($\alpha \in [0°, 360°]$), the width of stop band is enlarged, the peak of transmittance at the defect wavelength decreases, and the shape of transmittance near the defect wavelength becomes more narrow and sharp. In Figures 7(d)–(e), opposite observations for TM wave, however, are found. The contour plots of transmittance at normal and oblique incidence illustrate that adjusting the phase shift angle will provide more flexibility to fabricate narrow bandpass optical filters.

4. CONCLUSION

We have presented a detailed study of optical properties of a phase shift defect in a rugate structure under oblique incidence. When the angle of incidence increases, we find that: (1) the wavelength of the defect mode shifts to a shorter wavelength, (2) the stop band of the rugate structure moves toward a shorter wavelength region, (3) the bandwidth is enlarged for TE wave, but it is shortened for TM wave, (4) the full width at half maximum (FWHM) of the defect mode decreases for TE wave but it increases for TM wave, (5) the peak energy density increases and then drops for TE wave, while it always decreases for

TM wave. The overall views of transmittance contour plots for all possible phase shift angles (Figures 6 and 7) under both normal and oblique incidence and the energy density distribution at the defect wavelength (Figures 4 and 5) are useful for experimental designs of narrow bandpass filters and potential nonlinear optical applications. This study may provide a better understanding of designing narrow band filters or optical amplifiers based on one-dimensional continuous gradient-index optical materials.

ACKNOWLEDGMENT

REFERENCES

1. Joannopoulos, J. D., S. G. Johnson, J. N. Winn, and R. D. Meade, *Photonic Crystals: Modling the Flow of Light,* 2nd edition, Princeton University Press, 2008.

2. Awasthi, S. K., U. Malaviya, S. P. Ojha, N. K. Mishra, and B. Singh, "Design of a tunable polarizer using a one-dimensional nano-sized photonic bandgap structure," *Progress In Electromagnetics Research B*, Vol. 5, 133–152, 2008.

3. Banerjee, A., "Tunable polarizer using one-dimensional nano sized photonic bandgap structure," *Progress In Electromagnetics Research B*, Vol. 5, 133–152, 2008.

4. Golmohammadi, S., Y. Rouhani, K. Abbasian, and A. Rostami, "Photonic bandgaps in quasiperiordic multilayer using Fourier transform of the refractive index profile," *Progress In Electromagnetics Research B*, Vol. 18, 311–325, 2009.

5. Srivastava, R., S. Pati, and S. P. Ojha, "Enhancement of omnidirectional reflection in photonic crystals heterostructures," *Progress In Electromagnetics Research B*, Vol. 1, 197–208, 2008.

6. Srivastava, R., K. B. Thapa, S. Pati, and S. P. Ojha, "Omni-directional reflection in one-dimensional photonic crystals," *Progress In Electromagnetics Research B*, Vol. 7, 133–143, 2008.

7. Banerjee, A., "Enhanced temperature sensing by using one-dimensional ternary photonic band gap structures," *Progress In Electromagnetics Research Letters*, Vol. 11, 129–137, 2009.

8. Wu, C.-J. and Z.-H. Wang, "Properties of defect modes in one-dimensional photonic crystals," *Progress In Electromagnetics Research*, Vol. 103, 169–184, 2010.

9. Wu, C.-J., Y.-H. Chung, B.-J. Syu, and T.-J. Yang, "Band gap extension in a one-dimensional ternary metal-dielectric photonic crystal," *Progress In Electromagnetics Research*, Vol. 102, 81–93, 2010.

10. Rahimi, H., A. Namdar, S. Roshan Entezar, and H. Tajalli, "Photonic transmission spectra in one-dimensional fibonacci multilayer structures containing single-negative metamaterials," *Progress In Electromagnetics Research*, Vol. 102, 15–30, 2010.

11. Essadqui, A., J. Ben-Ali, D. Bria, B. Djafari-Rouhani, and A. Nougaoui, "Photonic band structure of 1D periodic composite system with left handed and right handed materials by green function approach," *Progress In Electromagnetics Research B*, Vol. 23, 229–249, 2010.

12. Deopura, M., C. K. Ullal, B. Temelkuran, and Y. Fink, "Dielectric omnidirectional visible reflector," *Opt. Lett.*, Vol. 26, 1197–1199, 2001.

13. Fink, Y., J. N. Winn, S. Fan, C. Chen, J. Michel, J. D. Joannopoulos, and E. L. Thomas, "A dielectric omnidirectional reflector," *Science*, Vol. 282, 1679–1682, 1998.

14. Winn, J. N., Y. Fink, S. Fan, and J. D. Joannopoulos, "Omnidirectional reflection from a one-dimensional photonic crystal," *Opt. Lett.*, Vol. 23, 1573–1575, 1998.

15. Van Popta, A. C., M. M. Hawkeye, J. C. Sit, and M. J. Brett, "Gradient-index narrow-bandpass filter fabricated with glancing-angle deposition," *Opt. Lett.*, Vol. 29, 2545–2547, 2004.

16. De Stefano, L., L. Moretti, A. Lamberti, O. Longo, M. Rocchia, A. M. Rossi, P. Arcari, and I. Rendina, "Optical sensors for vapors, liquids, and biological molecules based on porous silicon technology," *IEEE Trans. Nanotechnol.*, Vol. 543, 49–54, 2004.

17. Hawkeye, M. M., R. Joseph, J. C. Sit, and M. J. Brett, "Coupled defects in one-dimensional photonic crystal films fabricated with glancing angle deposition," *Opt Express*, Vol. 18, 13220–13226.

18. Hawkeye, M. M. and M. J. Brett, "Narrow bandpass optical optical filters fabricated with one-dimensionally periodic inhomogeneous thin films," *J. Appl. Phys.*, Vol. 100, 044322, 2006.

19. Hawkeye, M. M. and M. J. Brett, "Glancing angle deposition: Fabrication properties, and applications of micro- and nanostructured thin films," *J. Vac. Sci. Technol. A*, Vol. 25, 1317–1335, 2007.

20. Tabunshchyk, K. V., M. M. Hawkeye, A. Kovalenko, and M. J. Brett, "Three-dimensional simulation of periodically

structured thin films with uniaxial symmetry," *J. Phys. D: Appl. Phys.*, Vol. 40, 4936–4942, 2007.

21. Brett, M. J. and M. M. Hawkeye, "Materials science: New materials at a glance," *Science*, Vol. 319, 1192–1193, 2008.

22. Lu, Z., "Efficient 4×4 propagation matrix method using a fourth-order symplectic integrator for the optics of one-dimensional continuous inhomogeneous materials," *Progress In Electromagnetics Research Letters*, Vol. 14, 1–9, 2010.

23. Southwell, W. H., "Spectral response calculations of rugate filters using coupled-wave theory," *J. Opt. Soc. Am. A*, Vol. 5, 1558–1564, 1988.

24. Yeh, P., *Optical Waves in Layered Media*, John Wiley and Sons Ltd., New York, 1988.

25. Bovard, B. G., "Rugate filter theory: An overview," *Appl. Opt.*, Vol. 32, 5427–5442, 1993.

26. Abdulhalim, I., "Analytical propagtion matrix method for linear optics of arbitrary biaxial layered media," *J. Opt. A: Pure Appl. Opt.*, Vol. 1, 646–653, 1999.

27. Chin, S. A., "Symplectic integrators from composite operator factorizations," *Phys. Lett. A*, Vol. 226, 344–348, 1997.

28. Chin, S. A. and C. R. Chen, "Gradient symplectic algorithms for solving the Schrodinger equations with time-dependent potentials," *J. Chem. Phys.*, Vol. 117, 1409–1415, 2002.

29. Chin, S. A. and D. W. Kidwell, "Higher-order force gradient symplectic algorithms," *Phys. Rev. E*, Vol. 62, 8746–8752, 2000.

30. Berreman, D. W., "Optics in stratified and anisotropic media: 4×4 matrix formualtion," *J. Opt. Soc. Am.*, Vol. 62, 502–510, 1972.

31. Lu, Z., "Accurate and efficient calculation of light propagation in one-dimensional inhomogeneous anisotropic media through extrapolation," *J. Opt. Soc. Am A*, Vol. 24, 236–242, 2007.

32. Lu, Z., "Accurate calculation of reflectance spectra for thick one-dimensional inhomogeneous optical structures and media: Stable propagation matrix method," *Opt. Lett.*, Vol. 33, 1948–1950, 2008.

33. Suzuki, M., *Quantum Monte Carlo Methods in Condensed Matter Physics*, World Scientific Pub. Co. Inc., 1994.

34. Jin, J., *The Finite Element Method in Electromagnetics*, John Wiley and Sons Ltd., New York, 1993.